Artificial
Organs

Novel Fenestration Designs for Controlled Venous Flow Shunting in Failing Fontans With Systemic Venous Hypertension

*Priti G. Albal, *Prahlad G. Menon, *William Kowalski, †Akif Undar, ‡Riza Turkoz, and *§Kerem Pekkan

*Biomedical Engineering Department, Carnegie Mellon University, Pittsburgh; †Penn State Children's Hospital and Bioengineering, Pennsylvania State University, Hershey, PA, USA; ‡Cardiothoracic Surgery Department, Başkent University; and §Mechanical Engineering Department, Koc University, Istanbul, Turkey

Abstract: The Fontan procedure is employed as the final-stage palliation in single-ventricle congenital heart patients and results in diversion of venous blood directly to the pulmonary arteries. Fontan patients have been known to suffer from postoperative systemic venous hypertension, which in turn is associated with pleural effusions and protein losing enteropathy, leading to a decreased duration and quality of life. Despite the ongoing debate on its benefits, a circular fenestration hole (typically 4 mm) establishing a venous shunt to the common atrium is traditionally employed to relieve venous pressure in the Fontan conduit and improve early postoperative Fontan hemodynamics. However, these improvements come at the cost of reduced oxygen saturation due to excessive right-to-left shunting if the fenestration is permanent. The ideal "selective" fenestration would therefore limit or eliminate shunt flow at tolerable systemic venous pressures and allow increased flow at high pressures. The objective of this study is to introduce new fenestration designs that exhibit these desirable pressure-flow characteristics. Novel plus-shaped and S-shaped fenestration designs with leaflets are introduced as alternatives to the traditional circular fenestration, each having identical effective orifice areas at the fully open states. In vitro steady leakage flow tests were performed for physiological flow-driving pressures in order to obtain pressure-drop versus flow-rate characteristics. In addition, the leaflet opening kinematics of the plus-shaped fenestration was investigated computationally using finite element simulation. Fluid-structure interaction analysis was performed to determine leaflet displacements and pressure-flow characteristics at low pressures. Further, a lumped parameter model of the single-ventricle circuit was created to simulate pulsatile flow conditions For the plus-shaped fenestration, the flow rate was found to increase nonlinearly with increased driving systemic venous pressures at high physiological-pressure drops which did not cause the leaflets to fully open, and linearly for low driving pressures. These results indicate that leaflets of the plus-shaped fenestration design activated passively after a critical systemic venous pressure threshold. This feature is ideal for minimizing undesirable excessive venous shunting. A large variability in shunting flow rate may be obtained by changing the shape, thickness, size, and material of the fenestration to suit requirements of the patient, which can further limit shunt flow in a controlled manner. **Key Words:** Fontan surgery—Fenestration—Systemic venous hypertension—Venous flow shunting.

The Fontan operation is the primary surgical technique employed to palliate cyanotic congenital heart defects. The mixing of venous and arterial blood is eliminated by rerouting the caval flow directly to the pulmonary artery instead of through the common atrium (1–3). Since its introduction in 1971 (3), the Fontan operation has undergone several modifications (4,5). In cases of systemic venous hypertension (6), a fenestration hole is included in the Fontan connection for right-to-left flow shunting (7,8), therefore relieving the increased pressures similar to a pop-up valve. In an intracardiac (lateral tunnel) Fontan, the fenestration is placed in the intra-atrial baffle (9). In an extracardiac conduit Fontan, the fenestration is

doi:10.1111/aor.12011

Received July 2012; revised August 2012.

Address correspondence and reprint requests to Dr. Kerem Pekkan, Mechanical Engineering Department, Koc University, Rumelifeneri, Istanbul, Turkey. E-mail: kpekkan@ku.edu.tr

Presented in part at the 8th International Conference on Pediatric Mechanical Circulatory Support Systems and Pediatric Cardiopulmonary Perfusion held June 13–16, 2012 in Istanbul, Turkey.

First two authors contributed equally to this work.

generally placed by performing a 4–5-mm side-to-side anastomosis between the conduit and the right atrial free wall (10). The addition of a fenestration has been shown to decrease postoperative morbidity and mortality rates in high-risk patients (11). Further benefits of adding a fenestration is to improve CO as well as a lower incidence of protein-losing enteropathy, decreased pleural drainage, and shorter hospitalization time (7,8,12). However, these advantages come at the expense of lower systemic oxygenation, the theoretical risk of thromboembolism, reduced exercise capacity, and the potential need for intervention to close the fenestration (13). During follow-up studies, patients with fenestrated Fontan connections have been observed to have excessive right-to-left shunting due to insufficient resistance to flow at the fenestration (14,15). In spite of its clinical importance, the fenestration flow dynamics have not been investigated using state of the art bioengineering tools and generally ignored in computational congenital heart disease modeling studies.

The present study explores novel fenestration designs with a passive opening feature that has potential to mitigate excessive venous flow shunting at low systemic pressure levels. The focus of initial design efforts culminated in a four-leaflet (plus-shaped) baseline fenestration configuration as well as a novel S-shaped fenestration design, which offer greater pressure-driven shunt flow control. Fenestration leaflets offer resistance to outflow at low systemic venous pressures (<5 mm Hg) (9), and the passive leaflet function is designed to activate at venous pressures in excess of 5 mm Hg, therefore preventing excessive shunting through the fenestration.

MATERIALS AND METHODS

Fenestration geometry and prototypes

Fenestrations were constructed using material from a standard 22-mm polytetrafluoroethylene (PTFE) tube graft (Gore-Tex; W.L. Gore and Assoc, Flagstaff, AZ, USA) having a sheet thickness of 1/32″. Different incision shapes were made onto the PTFE sheet so as to create fenestrations having plus-shaped, S-shaped, and circular configurations. To create the plus-shape, two orthogonal 4-mm incisions were made, enclosing a small finite space between leaflets when in their closed position; this design is therefore referred to in this paper as the "4-mm plus-shaped" fenestration. To create the S-shape, two semicircular incisions of 1.6 mm were made to form an S-shape. The fully open effective orifice areas of all geometries are set to be equal. Figure 1 illustrates the tested fenestration configurations and depicts their respective closed and expected open states (with no buckling effects), when viewed normal to the outflow direction.

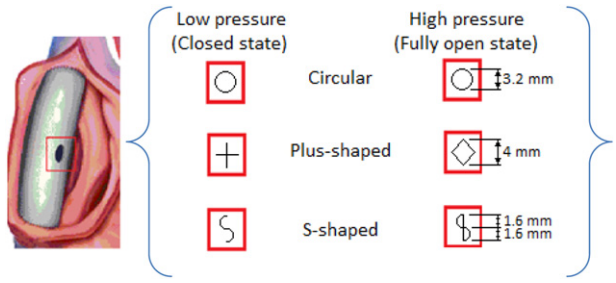

FIG. 1. Intra-atrial lateral tunnel Fontan conduit (left) showing a fenestration shunting venous flow to the atrium (adapted from [16]). Closed and idealized fully open configurations of different fenestration designs when viewed normal to the outflow direction are illustrated.

In vitro experimentation

For bench-top experiments, the PTFE sheet with the cutout fenestration was inserted between two tubes such that the fenestration was aligned with the center of the tube (Fig. 2b). Even though in the actual fenestration, dynamics are driven by static pressures acting at the Fontan conduit/baffle walls, in our experimental setup, fenestration dynamics were studied for leaflet opening using dynamic pressures encompassing the range of expected static pressures experienced by typical failing Fontan patients with hypertension. The leaflet dynamics are likely to remain similar in the patient-specific configuration.

Blood-analog glycerol with a dynamic viscosity of 3.2 mPa.s and density of 1060 kg/m^3 was used as the working fluid. The pressure head in the in vitro flow setup consists of a container calibrated to different pressures (by height of fluid column). This container was calibrated accurately and reliably using digital pressure sensors for pressures ranging from 3 mm Hg to 50 mm Hg. The container is connected to the fenestration through a tube, and the outlet is left open to atmospheric pressure. The latter represents the atrial pressure, that is, the reference pressure for this flow setup (zero gauge pressure). The flow setup is illustrated in Fig. 2a. In order to obtain the required upstream pressure, Hoffman clamps were employed at the outflow side until the overall pressure in the circuit increased. The clamp was subsequently removed for measurement of pressure and flow rate as the flow past the fenestration is stabilized. Four readings were taken for every pressure setting.

Pressure was measured upstream close to the fenestration (about 5 equivalent diameters) and far

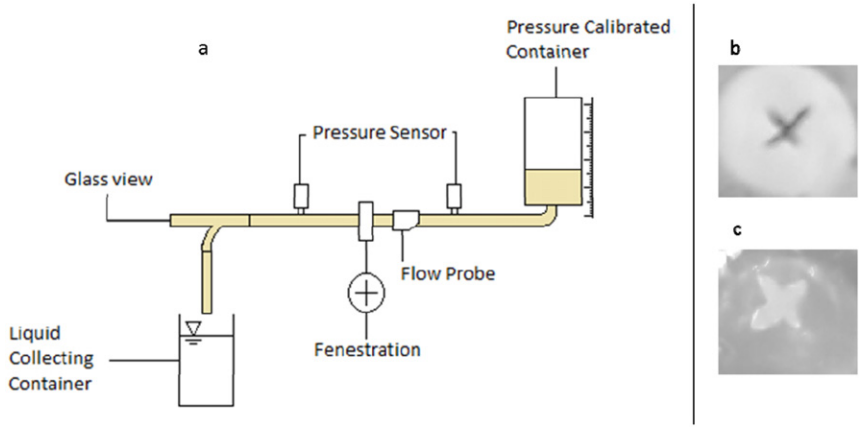

FIG. 2. In vitro experimental test rig. (a) Schematic of experimental setup including a pressure calibrated container, a PTFE sheet with the fenestration, glass view to record leaflet kinematics, flow sensors to measure flow rate through the fenestration, and pressure sensors to measure upstream/downstream pressure. (b) PTFE sheet with a 4-mm plus-shaped fenestration coaxially inserted between a transparent tubing pair. (c) Fenestration opening at 25 mm Hg of pressure.

downstream (>50 equivalent diameters) of the fenestration hole using TruWave disposable pressure transducers (Edwards Life Sciences, Irvine, CA, USA) attached to a multichannel differential amplifier (WPI, Inc., Sarasota, FL, USA) in full bridge configuration. Flow rate thorough the tube was measured using transonic flow probes (6XL and 9XL, Transonic, Inc., Ithaca, NY, USA). A dedicated data acquisition module NI USB-229 (NI, Inc., Austin, TX, USA) with 16-bit resolution and multiplexing capabilities was employed for sampling and recording data at 100 Hz. The experiments were performed for plus-shaped, S-shaped, and circular type fenestration designs in order to compare their outflow characteristics. A glass-viewing window was placed just before the outlet of the setup in order to observe the dynamics of leaflet opening for increasing venous pressures (17).

Fluid-structure interaction (FSI) model

In order to acquire the detailed three-dimensional (3D) leaflet shape and effective orifice area, a finite element computer model of the 4-mm plus-shaped fenestration, as in the experimental setup, was developed using the Parasolid geometry engine within ADINA software (Watertown, MA, USA). The four leaflets of the plus-shaped fenestration were approximately quadrants enclosing a rest state opening of 0.84 mm^2. The thickness of the leaflets was considered as 100 µm. FSI simulations were conducted using the finite element technique considering 3D solid elements for the leaflets with mechanical properties of PTFE (Young's Modulus: 0.55 mPa, density: 2160 kg/m^3), under assumptions of small-displacement constituent formulation and linear, elastic, and isotropic material properties. PTFE was modeled as an elastic incompressible material for only small strain. The finite element volumetric mesh was composed of ~3300 3D solid elements (10 nodes per element). Fixed boundary conditions were applied at the circumferential surfaces of the fenestration. All fluid contacting surfaces were specified as flow structure interaction surfaces.

The fluid model (Fig. 3b) was created by performing a Boolean subtraction operation of the fenestration from a tube of 5 mm diameter such that the fenestration was positioned normal to the flow in the cylinder, similar to experimental conditions. The finite element model for the fluid domain consisted of ~250 000 tetrahedral elements. The fluid was modeled

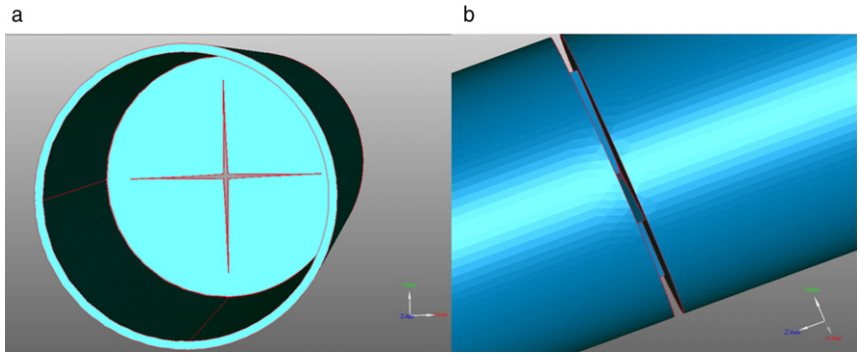

FIG. 3. (a) Solid model of a 4-mm plus-shaped fenestration positioned normal to a cylindrical tube having 5 mm inner diameter. (b) Fluid region of the leaflet model for FSI created by performing a Boolean subtraction operation from a tube of 5 mm inner diameter.

as an incompressible laminar viscous fluid with constant properties ($\mu = 3.71$ mPa.s, $\rho = 1060$ kg/m^3). Displacement compatibility and traction equilibrium along the structure-fluid interfaces were satisfied by iterative FSI coupling. Normal traction boundary conditions were applied at inlet and outlet faces of the fluid model (zero traction enforced at outlet).

Transient FSI simulations using ADINA were conducted to simulate leaflet opening for different inlet face pressures encompassing a range that induced small displacements in the immersed leaflets. The mesh density of the fluid and solid models were arrived at by trial and error in order to ensure that overlapping elements did not occur at any point during the simulation. To verify these results, a coarse one-way fluid-to-solid coupled simulation was conducted in ANSYS Workbench 14 (ANSYS, Inc., Canonsburg, PA, USA) by coupling a fluid model in ANSYS Fluent with the static structural model in ANSYS Mechanical, also employing the small-displacement formulation and linear, elastic, isotropic material properties. A two-way coupled FSI simulation considering a nonlinear, large-displacement, elastic constituent formulation with isotropic material properties was also conducted in ANSYS Workbench 14 to estimate more realistic leaflet displacement values at low fluid pressures. The volumetric fluid mesh comprised of 70 000 tetrahedral elements and the solid fenestration leaflets was composed of 200 hexahedral elements.

For large leaflet displacements in thick leaflets, transient opening of the leaflets was verified using a simple solid mechanics model (300 shell element, 1020 nodes) having a shell finite element formulation. The shell element model is ideal for large displacements and rotations but small strains, for the same mechanical and material properties with a shell thickness of 1000 μm. Pressure loading was applied normal to the fenestration as well as radially outwards. Linearly increasing pressure loading was applied to compute the time-resolved leaflet displacements and open leaflet shape configuration similar to our observations from the viewing window in our in vitro experiments.

Lumped parameter modeling—experiment verification for pulsatile flow

In order to verify experimental pressure-drop versus flow-rate characteristics and also examine effects of flow pulsatility at the circulation system level, we simulated an electric circuit analog of the single ventricle (SV) cardiovascular system using a lumped parameter model (LPM) previously developed by our group (18,19). This model is similar to the formulation described by Peskin and Tu (20) and has been used extensively to study normal and diseased patient cardiovascular configurations (18,20,21). In this model, arteries, veins, and ventricles are treated as pure time-dependent compliance chambers with lumped capillary and valve resistances. The instantaneous flow and pressure from chamber i to chamber j are evaluated by solving the following set of differential equations:

$$Q_{ij} = (P_j - P_i) * \frac{1}{R_{ij}} * S_{ij} \quad (1)$$

$$\frac{d(C_i P_i)}{dt} = \sum_{j-1}^{N} (Q_{ij} - Q_{ji}) \quad (2)$$

P_i, Q_i, and C_i are the pressures, flows, and compliances in chamber i; R_{ij} and S_{ij} are the resistances and switches enforcing the directionality of flows, respectively. The differential equation was solved iteratively for each chamber until pressure convergence.

We adapted our previous baseline model of the SV physiology to include a fenestration connection (Fig. 4). In the basic SV circuit, there is a chamber for the SV, systemic artery bed (SAB), systemic venous bed (SVB), pulmonary artery bed (PAB), pulmonary venous bed (PVB), and common atrium (SA), i.e. $n = 6$. Each of these chambers had compliance and resistance components. The total cavopulmonary connection (TCPC) is treated as a serial resistance within the SVB chamber, such that the total resistance to flow between the SVB and PAB compliance components is $R_{SVB} + R_{TCPC}$ in series. The fenestration is treated similarly, acting as a serial resistance between the SVB and SA compliance components (Fig. 4). The parameters governing the systemic and pulmonary circulations were calibrated to produce 3.8 L/min cardiac output (CO), with a mean arterial pressure (MAP) and mean pulmonary artery pressure (PAP) of 96 and 7 mm Hg, respectively. These values were based on clinical data obtained from cardiac catheterization (22). Common atria and ventricles were modeled as time-varying compliance chambers where pulsatile pressure was generated via functions that alternate between systolic (stiff) and diastolic (relaxed) ventricular properties. These activation functions govern the systolic and diastolic contraction of the myocardial muscle. The compliance values were computed from the following equations:

$$E(t) = \frac{1 - e^{-\frac{t}{T_C}}}{1 - e^{-\frac{T_S}{T_C}}} \quad 0 \le t \le T_S \quad (3)$$

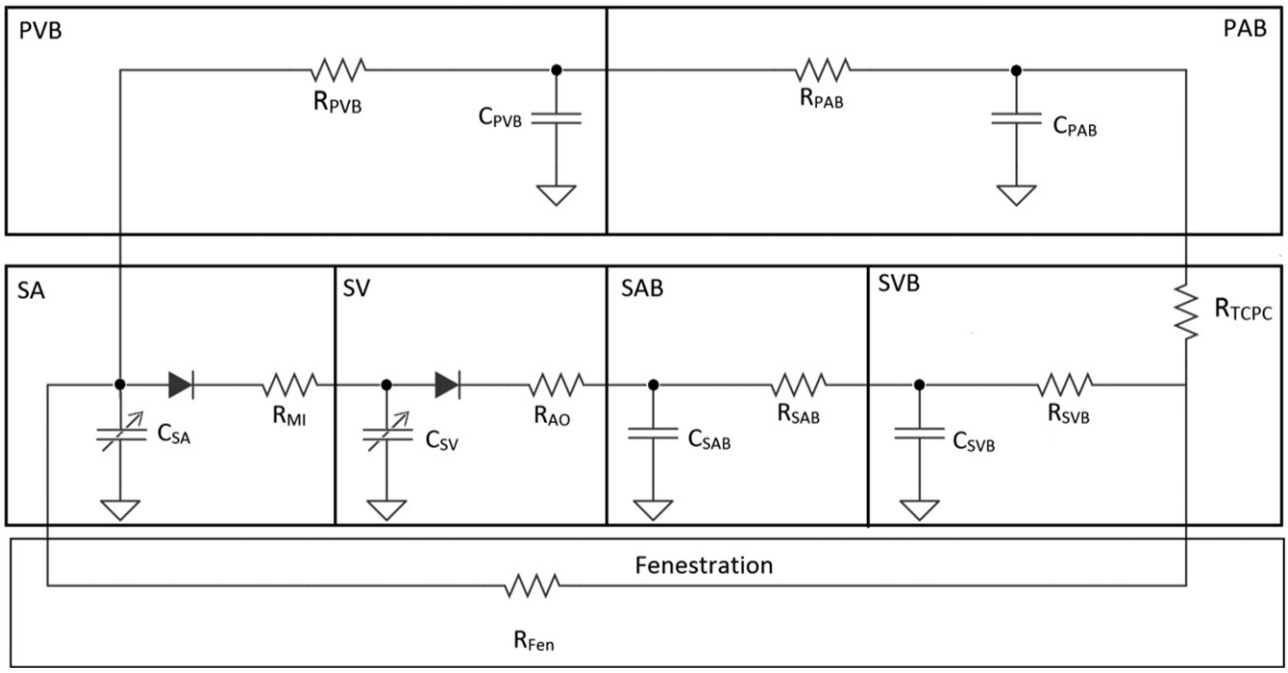

FIG. 4. Schematic of the single-ventricle, lumped parameter model circuit with fenestration. PVB, pulmonary venous bed; PAB, pulmonary artery bed; SA, single atrium; SV, single ventricle; SAB, systemic artery bed; SVB, systemic venous bed; TCPC, total cavopulmonary connection; MI, mitral valve; AO, aortic valve; R, resistance; C, compliance.

$$CV(t) = CVD \cdot \left(\frac{CVS}{CVD} \right)^{E(t)} \tag{4}$$

$$E(t) = \frac{1 - e^{-\frac{t - T_S}{T_R}}}{1 - e^{-\frac{T - T_S}{T_R}}} \quad T_S \le t \le T \tag{5}$$

$$CV(t) = CVS \cdot \left(\frac{CVD}{CVS} \right)^{E(t)} \tag{6}$$

where E is the load of each chamber, T_C (0.0025 min) and T_R (0.00075 min) are the time constants governing the contraction and relaxation of the myocardial muscle during systole and diastole. T is the duration of one cardiac cycle (1/heart rate), T_S is the length of systole (T/3), and t is the current point in the cardiac cycle. Systole and diastole were switched for modeling atrial contraction. CVD and CVS were the minimum and maximum compliance values of the chamber. Mitral (R_{MI}) and aortic (R_{AO}) valve resistances were assigned values of 0.01 mm Hg/(L/min) in the forward flow direction and infinite resistance in the reverse direction to model one-way flows. We assigned a heart rate of 70 bpm, modeling a resting state. Central venous pressure (CVP) was varied from 7 to 33 mm Hg, encompassing normal to hypertensive cases. For each CVP, R_{SAB}, and R_{SVB} were adjusted to maintain the CO, MAP, and PAP listed previously. We considered a CVP of 13 mm Hg as the baseline model, with parameters given in Tables 1a,b.

The 3.2-mm-diameter circular fenestration and the proposed plus-shaped design is simulated by changing the fenestration resistance (R_{fen}) as per the experimentally determined pressure-flow characteristics. To model a circular fenestration, we applied a constant resistance value of 16 mm Hg/(L/min),

TABLE 1a. *Parameters used in the lumped parameter analysis for the single-ventricle circulation*

LPM parameters for systemic and pulmonary circulation	
Compliance (L/mm Hg)	
C_{SAB}	0.001
C_{SVB}	0.3325
C_{PAB}	0.00412
C_{PVB}	0.08
Resistance (mm Hg/(L/min))	
R_{SAB}	19.5
R_{SVB}	3.04
R_{PAB}	0.8
R_{PVB}	0.11
R_{TCPC}	0.39

PVB, pulmonary venous bed; PAB, pulmonary artery bed; SAB, systemic artery bed; SVB, systemic venous bed; TCPC, total cavopulmonary connection; R, resistance; C, compliance.

TABLE 1b. *Parameters used in the lumped parameter analysis for the single ventricle*

LPM parameters for single ventricle	
Compliance (L/mm Hg)	
CVD_{SV}	0.0146
CVS_{SV}	0.00003
CVD_{SA}	0.001
CVS_{SA}	0.0003
Resistance (mm Hg/(L/min)	
R_{MI}	0.01
R_{AO}	0.01

SA, single atrium; SV, single ventricle; MI, mitral valve; AO, aortic valve; R, resistance; CVS, minimum compliance values of the chamber; CVD, maximum compliance values of the chamber.

which was computed by fitting a straight line to our in vitro test data. The nonlinear pressure-flow characteristics due to effects of leaflet opening in the new plus-shaped designs required R_{fen} to vary with the pressure drop across the fenestration. Flow through the fenestration and the pulmonary to systemic flow ratio (Qp/Qs) were compared over the CVP pressure range to determine the effects of our plus-shaped design. Q_P/Q_S served as an index for systemic oxygen delivery and is a major factor in patient survival (22,23).

RESULTS AND DISCUSSION

In vitro experimentation

Measured and computed venous pressure versus flow-rate characteristic curves were plotted to encompass the possible range of leaflet motion and pressure (Fig. 5). Through this plot, it was possible to quantitatively determine the operational pressure ranges of the new fenestration design and its passive function in mitigating excessive shunting when compared with a standard circular fenestration without leaflets. All results were dynamically scaled in order to compute equivalent pressure drop versus flow rate of blood. Downstream flow rates for the circular fenestrations increased linearly with pressure drop at physiological pressures (3–30 mm Hg) and matched theoretical Poiseulle flow values. At higher pressures (>30 mm Hg), the venturi effect due to the centrally located fenestration in the tubing of the experimental setup became more pronounced. In contrast, the pressure-flow characteristics for the 4-mm plus-shaped fenestration were fit to a nonlinear second degree polynomial. At pressures lower than 5 mm Hg the flow rate could be approximated to hold a linear relationship with pressure, due to limited leaflet motion, that is, leaflets remained at a state of quasi-equilibrium until a critical threshold pressure drop beyond which leaflet opening became more significant. This is further adjusted with the choice of material. The pressure-flow characteristics far downstream for the S-shaped fenestration fit to a second degree polynomial curve as well and were observed to have similar effectiveness as the plus-shaped design in mitigating shunting at low pressures. At higher pressures (5–50 mm Hg), leaflets were observed to begin opening more completely therefore causing flow rate to increase nonlinearly with change in pressure, on account of a changing effective orifice area. The S-shaped fenestration performed better at avoiding low-pressure shunting flow, because it had lesser open area at rest state in comparison with the 4-mm plus-shaped fenestration. At very high pressures, the flow characteristics for both plus-shaped and S-shaped fenestrations became linear due to complete opening of fenestration leaflets.

FSI model

Shunting flow rates and leaflet displacements observed at extremely low venous pressures (1–3 mm Hg) were possible to determine from the FSI modeling whereas flow at higher pressure was found from in vitro experiments. Numerical modeling allowed us to examine the fenestration leaflet kinematics during the opening process in 3D using FSI for 100-μm thick leaflets. Similar pressure–flow rate characteristics were obtained from ADINA as well as ANSYS one-way coupled and two-way coupled simulations for the modeled driving pressure range, although different leaflet displacement values were observed between small and large displacement constituent formulations, as expected. The maximum displacement simulated with the ADINA FSI model for

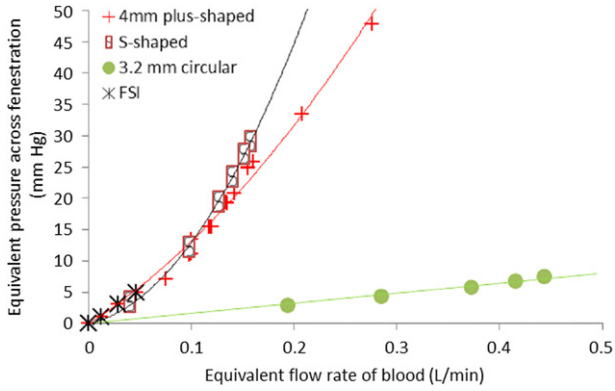

FIG. 5. Pressure-drop versus flow-rate characteristics for a 4-mm plus-shaped fenestration (red +) plotted along with results from ADINA FSI modeling (black *) at low pressure drops during the opening phases of the fenestration. Characteristic curves for a 3.2-mm circular fenestration (green) and S-shaped fenestration (black) are also plotted.

3 mm Hg pressure drop was 0.13 mm and comparable displacement values were obtained from ANSYS one-way coupled FSI simulations (Fig. 6). Nonlinear buckling is not modeled in these two cases. However, for a pressure drop of 10 mm Hg, a peak displacement was 0.67 mm using the small-displacement models, whereas the same peak displacement was reported in the two-way coupled model for a lower fluid driving pressure (~0.1 mm Hg). This discrepancy is due to the fact that a thinner 100-μm leaflet was modeled and the large-displacement model considered nonlinear structural effects. These displacement values are likely to be more realistic; however, in our experiments, thicker (~770 μm thick) leaflets were used, which are likely to have been structurally displaced relatively less.

The loading conditions for this model are analogous to a cantilever beam with varying area of cross section under uniformly distributed load conditions. In the analytical solution for displacement (δ) by the cantilever analogy for leaflet motion, δ is directly related to the point loading force (F) applied and the cube of the length of beam (i.e., the span/radius of the leaflets, L), but inversely related to the modulus of elasticity (E) and area moment of inertia of the leaflet cross section (I), that is, $\delta = \frac{FL^3}{3EI}$. Since the leaflet cross section is best approximated as a rectangle of varying area from base to tip of the leaflet, area moment of inertia is expected to be related to the cube of the leaflet thickness. Applying the cantilever analogy for leaflet motion to the nonlinear FSI result, for about 10 mm Hg (i.e., 100× the nonlinear FSI model loading conditions) considering 770-μm thick leaflets, the expected displacement along the direction of the cylindrical tube would be ~0.2 mm. Therefore, at 25 mm Hg, a 0.5 mm displacement is expected, which is comparable with our experimental observations. Therefore, although the FSI models were all proficient at obtaining pressure-flow characteristics, the leaflet displacement predictions and the choice of material models requires more thorough experimental validation. This may be achieved by experimental time-resolved 3D leaflet motion studies in future.

At small leaflet sizes, operation without nonlinear leaflet structural movement or buckling is a desirable characteristic for minimizing excessive venous shunting at lower pressures; however, at high pressures, leaflet buckling might be unavoidable. The buckling potential of leaflets is expected to be a function of leaflet size and leaflet aspect ratio. Minor deviations of FSI pressure-flow results (see Fig. 5) from experimental trends may be accounted for due to possible differences between the mechanical properties modeled using finite element analysis and the true experimental leaflet material.

The shell-based formulation of transient solid mechanics of the fenestration leaflets helped reveal the 3D surfaces expected during leaflet opening (see Fig. 7). Leaflet displacement was found to have an inverse relationship with thickness of leaflets, similar to predictions from the cantilever analogy. Therefore, leaflet sensitivity to systemic venous pressure may be designed by an appropriate adjustment of leaflet thickness.

Lumped parameter modeling

Values for the baseline LPM case, with CVP of 13 mm Hg, were compared with our experimental results to verify performance of the flow loop. The average pressure drop across the fenestration over the cardiac cycle was 9 mm Hg, and average flow through the fenestration was 76 mL/min for the circular fenestration and 52.8 mL/min for the plus-shaped design. These flow values are nearly identical to those measured experimentally for the same pressure drop as expected (Fig. 5). CVP was then varied from 7 to 33 mm Hg. As CVP increased, so did the resistance of the plus-shaped fenestration, according to the relationship in Fig. 8a. Flow rate through the fenestration was considerably less at higher CVP (>5 mm Hg), due to the increased resistance at higher pressures (Fig. 8b). The variation in pressure drop across the fenestration observed during pulsatile flow conditions (Fig. 8d) remained approximately the same regardless of the shape (circular or plus-shaped) in the LPM. The dynamic resistance of the plus-shaped fenestration provided as an input to the LPM was associated with the variations observed in the fenestration flow rate at the same effective orifice area. The varying resistance offered by virtue of opening leaflets of the plus-shaped fenestration manifested itself in the corresponding flow-rate waveforms in the form of a diminished difference between minimum and maximum recorded flow rates over a cardiac cycle (0.01 L/min), in comparison with the 3.2-mm circular fenestration (0.08 L/min). The mere presence of the leaflets themselves led to an overall increased resistance to shunting flow, which resulted in decreased mean flow across the plus-shaped fenestration, in comparison with the equivalent circular shape. This feature of the new plus-shaped design is desirable, as it reduces right-left shunting at hypertensive CVP. The reduction in Q_p/Q_s at higher CVP was less dramatic for the plus-shaped versus circular fenestration shape (Fig. 8c).

Immediately postoperative to Fontan surgeries involving a cardiopulmonary bypass, pulmonary

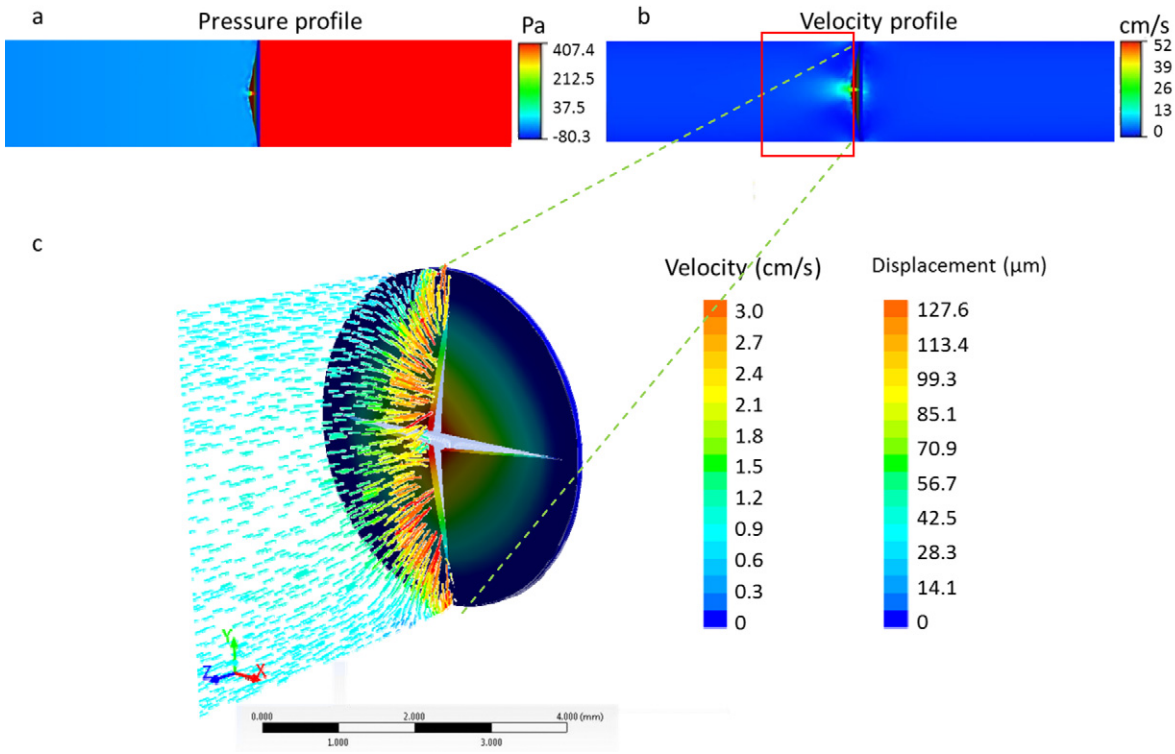

FIG. 6. Applied pressure gradient (a) and corresponding longitudinal velocity profile (b), as obtained from ADINA FSI modeling for small leaflet displacements of a 4-mm plus-shaped fenestration. (c) Magnified velocity vectors colored by scaled velocity magnitude in a longitudinal slice through fenestration as obtained from ANSYS simulation for a two-way coupled large-displacement model, for the same pressure drop. Fenestration surfaces are colored by magnitude of total displacement along the axis of the pipe.

vascular resistance is high, which leads to an increased systemic venous pressure. Given the pressure-controlled shunting flow that the new fenestration designs offered, a four-leaflet, plus-shaped fenestration or a bi-leaflet, S-shaped design similar to the ones tested in this study may be integrated with the standard Fontan conduit design in order to relieve high postoperative venous pressures in the

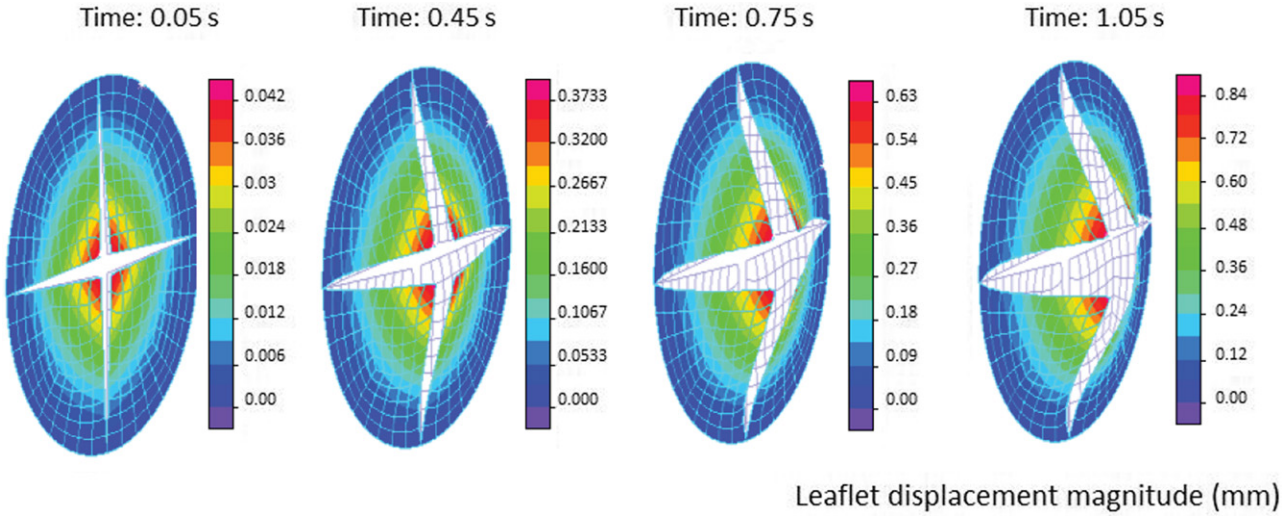

FIG. 7. Opening of leaflets simulated with shell-solid mechanics subject to simulated pressure loading. Magnitude of total displacement colored on the fenestration surface.

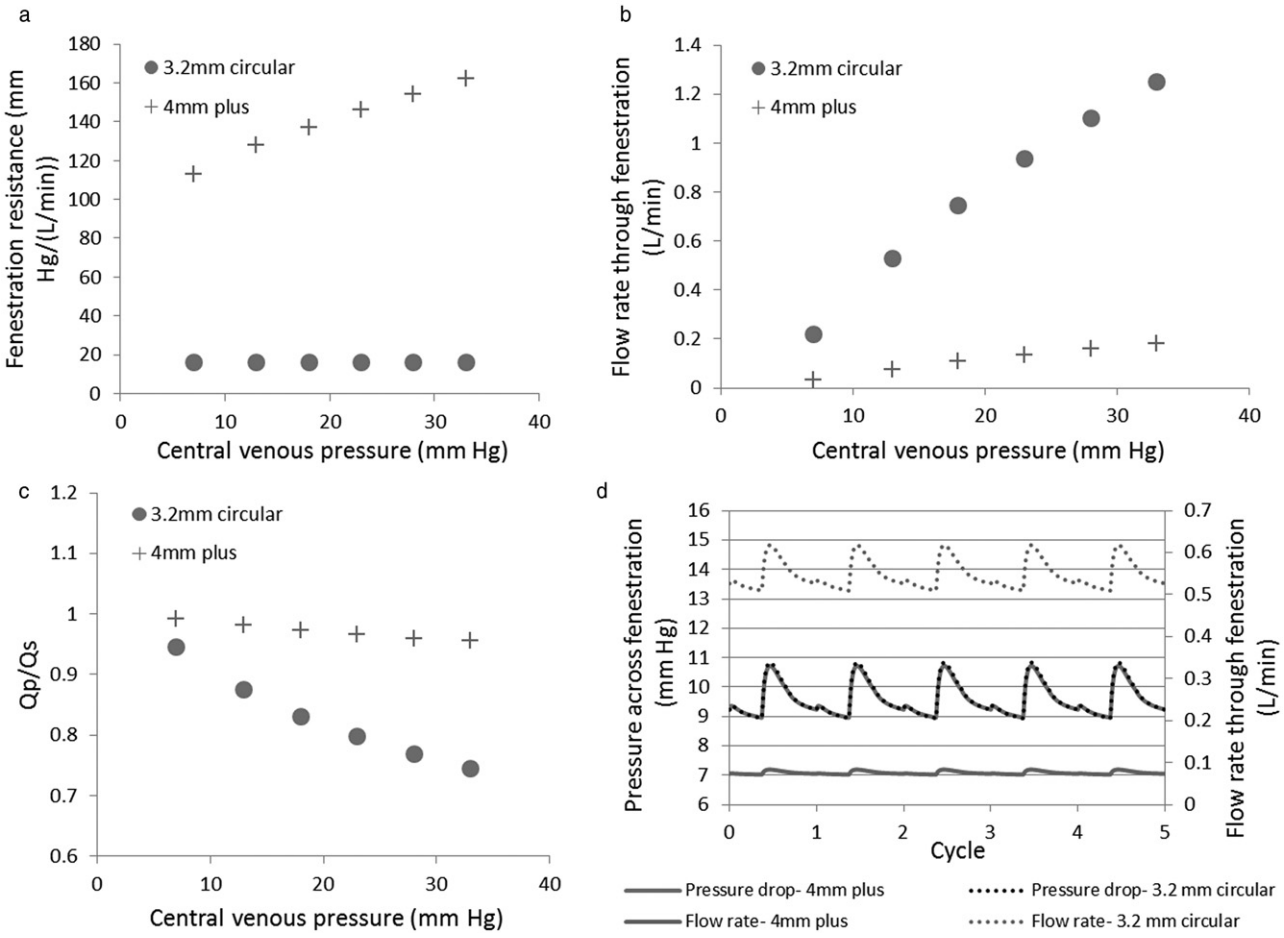

FIG. 8. Pulsatile hemodynamic results obtained from LPM. (a) Fenestration resistance versus central venous pressure for a 4-mm plus-shaped and 3.2-mm circular fenestration. The circular fenestration has a constant resistance of 16 mm Hg/(L/min) as specified from experiments. Resistance of a 4-mm plus-shaped fenestration is modeled as a nonlinear function of change in pressure drop across the fenestration (b) Flow rate versus central venous pressure for a 4-mm plus-shaped fenestration and 3.2-mm circular fenestration. (c) Ratio of pulmonary flow rate and systemic flow rate versus central venous pressure. (d) Pulsatile flow rate across the different fenestrations (having the same effective orifice area) for the same pulsatile pressure gradient waveform plotted over five cardiac cycles.

Fontan connection while simultaneously limiting excessive shunting at low pressures. This may also help in controlling hypoxia. Another benefit of the leaflets is their potential for spontaneous closure by virtue of neointimal formation at the leaflet boundaries, when the systemic venous pressures are consistently low enough to insufficiently open the leaflets. Tissue-engineered Fontan grafts (23) have indicated likelihood of self-endothelialization in recent clinical studies (24) and therefore could be explored as a promising alternative material.

Thrombus formation at the leaflets proposed in the new fenestration designs is an important criterion for the design of new fenestrations with leaflets that could not be evaluated with the blood-analog experiments reported in this study. Thrombogenesis may potentially be a fatal complication and studies conducted on prosthetic heart valves have indicated that such incidents may occur as high as 20% of the time for right heart prostheses, although thrombogenic events have been reported to be rarer in left heart prostheses (25). In order to mitigate such risks at the proposed fenestration leaflets, further in vitro experimental tests with blood are therefore strongly warranted. Likewise, regular echocardiography evaluations are also needed for complete hemodynamic performance analysis of the new fenestrated Fontan conduits employing leaflet designs. Pulsatile fenestration flow will establish good leaflet mobility and may reduce thrombogenic risk.

CONCLUSION

Although there are advantages of introducing a fenestration in a failing Fontan, excessive venous flow shunting is undesirable. The new fenestration

proposed in this study is an alternative to overcome this limitation by mitigating controlled shunting at low pressures using passive leaflet designs. Hence, this fenestration configuration may be adopted as part of a standard Fontan conduit for pressure-controlled shunting functionality, pending standard blood damage and thromogenesis assessment. To achieve the desired patient-specific opening and flow characteristics, it is further possible to modify the fenestration design by altering size, thickness, and material of the leaflets. The leaflets in the proposed fenestration designs may potentially facilitate spontaneous and permanent leaflet closure by neointimal formation when systemic venous pressures are consistently low enough. Present studies are focused at analyzing the several different fenestration design concepts in order to seek an optimal leaflet shape and configuration offering minimum orifice area at rest state and more precise control over leaflet-activation pressures for improved control over shunting flow functionality and tailoring for patient-specific situations. Experimental observation of leaflet opening for each of the tested fenestration configurations using stereoscopic imaging techniques is necessary in order to fully validate preliminary computational models.

REFERENCES

1. Rychik J, Rome JJ, Jacobs ML. Late surgical fenestration for complications after the Fontan operation. *Circulation* 1997;96:33–6.
2. Giannico S, Hammad F, Amodeo A, et al. Clinical outcome of 193 extracardiac Fontan patients: the first 15 years. *J Am Coll Cardiol* 2006;47:2065–73.
3. Fontan F, Baudet E. Surgical repair of tricuspid atresia. *Thorax* 1971;26:240–8.
4. Soerensen DD, Pekkan K, de Zélicourt D, et al. Introduction of a new optimized total cavopulmonary connection. *Ann Thorac Surg* 2007;83:2182–90.
5. de Leval MR, Kilner P, Gewillig M, Bull C. Total cavopulmonary connection: a logical alternative to atriopulmonary connection for complex Fontan operations. Experimental studies and early clinical experience. *J Thorac Cardiovasc Surg* 1988;96:682–95.
6. Laks H, Pearl JM, Haas GS, et al. Partial Fontan: advantages of an adjustable interatrial communication. *Ann Thorac Surg* 1991;52:1084–94; discussion 1094–5.
7. Bridges ND, Lock JE, Castaneda AR. Baffle fenestration with subsequent transcatheter closure. Modification of the Fontan operation for patients at increased risk. *Circulation* 1990; 82:1681–9.
8. Bridges ND, Mayer JE Jr, Lock JE, et al. Effect of baffle fenestration on outcome of the modified Fontan operation. *Circulation* 1992;86:1762–9.
9. Kuhn MA, Jarmakani JM, Laks H, et al. Effect of late postoperative atrial septal defect closure on hemodynamic function in patients with a lateral tunnel Fontan procedure. *J Am Coll Cardiol* 1995;26:259–65.
10. Thompson LD, Petrossian E, McElhinney DB, et al. Is it necessary to routinely fenestrate an extracardiac Fontan? *J Am Coll Cardiol* 1999;34:539–44.
11. Hsia TY, Khambadkone S, Redington AN, de Leval MR. Effect of fenestration on the sub-diaphragmatic venous hemodynamics in the total-cavopulmonary connection. *Eur J Cardiothorac Surg* 2001;19:785–92.
12. Ono M, Boethig D, Goerler H, Lange M, Westhoff-Bleck M, Breymann T. Clinical outcome of patients 20 years after Fontan operation—effect of fenestration on late morbidity. *Eur J Cardiothorac Surg* 2006;30:923–9.
13. Lemler MS, Scott WA, Leonard SR, Stromberg D, Ramaciotti C. Fenestration improves clinical outcome of the Fontan procedure: a prospective, randomized study. *Circulation* 2002; 105:207–12.
14. Sommer RJ, Recto M, Golinko RJ, Griepp RB. Transcatheter coil occlusion of surgical fenestration after Fontan operation. *Circulation* 1996;94:249–52.
15. Laks H. The partial Fontan procedure. A new concept and its clinical application. *Circulation* 1990;82:1866–7.
16. Gaca AM, Jaggers JJ, Dudley LT, Bisset GS 3rd. Repair of congenital heart disease: a primer—part 1. *Radiology* 2008; 247:617–31.
17. Dur O, Yoshida M, Manor P, et al. In vitro evaluation of right ventricular outflow tract reconstruction with bicuspid valved polytetrafluoroethylene conduit. *Artif Organs* 2010;34:1010–6.
18. Pekkan K, Frakes D, De Zelicourt D, Lucas CW, Parks WJ, Yoganathan AP. Coupling pediatric ventricle assist devices to the Fontan circulation: simulations with a lumped-parameter model. *ASAIO J* 2005;51:618–28.
19. Kowalski WJ, Dur O, Pekkan K. A lumped parameter model for the measurement of O2 and CO2 concentration in congenital heart defects, in *BMES Annual Fall Meeting*. Austin, TX. 2010.
20. Peskin CS, Tu C. Hemodynamics in congenital heart disease. *Comput Biol Med* 1986;16:331–59.
21. Sun Y, Beshara M, Lucariello RJ, Chiaramida SA. A comprehensive model for right-left heart interaction under the influence of pericardium and baroreflex. *Am J Physiol* 1997;272(3 Pt 2):H1499–515.
22. Sundareswaran KS, Pekkan K, Dasi LP, et al. The total cavopulmonary connection resistance: a significant impact on single ventricle hemodynamics at rest and exercise. *Am J Physiol Heart Circ Physiol* 2008;295:H2427–35.
23. Hibino N, Duncan DR, Nalbandian A, et al. Evaluation of the use of an induced puripotent stem cell sheet for the construction of tissue-engineered vascular grafts. *J Thorac Cardiovasc Surg* 2012;143:696–703.
24. Patterson JT, Gilliland T, Maxfield MW, et al. Tissue-engineered vascular grafts for use in the treatment of congenital heart disease: from the bench to the clinic and back again. *Regen Med* 2012;7:409–19.
25. Sullivan MM, Theleman KP, Choi JW. Percutaneous closure of patent ductus arteriosus in an asymptomatic adult. *Proc (Bayl Univ Med Cent)* 2008;21:386–8.